Wafer-scale heterogeneous integration InP on trenched Si with a bubble-free interface

APL Materials

Wafer-scale heterogeneous integration InP on trenched Si with a bubble-free interface

Cite as: APL Mater. 8, 051110 (2020); https://doi.org/10.1063/5.0004427
Submitted: 11 February 2020 . Accepted: 03 May 2020 . Published Online: 19 May 2020

Jiajie Lin, Tiangui You, Tingting Jin, Hao Liang, Wenjian Wan, Hao Huang, Min Zhou, Fengwen Mu, Youquan Yan, Kai Huang, Xiaomeng Zhao, Jiaxiang Zhang, Shumin Wang, Peng Gao, and Xin Ou

AIP Publishing

Wafer-scale heterogeneous integration InP on trenched Si with a bubble-free interface

Cite as: APL Mater. 8, 051110 (2020); doi: 10.1063/5.0004427
Submitted: 11 February 2020 • Accepted: 3 May 2020 •
Published Online: 19 May 2020

Jiajie Lin,[1,2] Tiangui You,[1] Tingting Jin,[1,2] Hao Liang,[1,2] Wenjian Wan,[3] Hao Huang,[1,4] Min Zhou,[1] Fengwen Mu,[5] Youquan Yan,[1,2] Kai Huang,[1] Xiaomeng Zhao,[1] Jiaxiang Zhang,[1] Shumin Wang,[6] Peng Gao,[7] and Xin Ou[1,2,a)]

AFFILIATIONS

[1]State Key Laboratory of Functional Materials for Informatics, Shanghai Institute of Microsystem and Information Technology, Chinese Academy of Sciences, 865 Changning Road, Shanghai 200050, China
[2]Center of Materials Science and Optoelectronics Engineering, University of Chinese Academy of Sciences, Beijing 100049, China
[3]Key Laboratory of Terahertz Solid-State Technology, Shanghai Institute of Microsystem and Information Technology, Chinese Academy of Sciences, 865 Changning Road, Shanghai 200050, China
[4]School of Physical Science and Technology, Shanghai Tech University, Shanghai 201210, China
[5]Kagami Memorial Research Institute for Materials Science and Technology, Waseda University, Shinjuku, Tokyo 169-0051, Japan
[6]Department of Microtechnology and Nanoscience, Chalmers University of Technology, Gothenburg 41296, Sweden
[7]Science and Technology on Power Sources Laboratory, Tianjin Institute of Power Sources, Tianjin 300384, China

[a)]**Author to whom correspondence should be addressed:** ouxin@mail.sim.ac.cn

ABSTRACT

Heterogeneous integration of compound semiconductors on a Si platform leads to advanced device applications in the field of Si photonics and high frequency electronics. However, the unavoidable bubbles formed at the bonding interface are detrimental for achieving a high yield of dissimilar semiconductor integration by the direct wafer bonding technology. In this work, lateral outgassing surface trenches (LOTs) are introduced to efficiently inhibit the bubbles. It is found that the chemical reactions in InP–Si bonding are similar to those in Si–Si bonding, and the generated gas can escape via the LOTs. The outgassing efficiency is dominated by LOTs' spacing, and moreover, the relationship between bubble formation and the LOT's structure is well described by a thermodynamic model. With the method explored in this work, a 2-in. bubble-free crystalline InP thin film integrated on the Si substrate with LOTs is obtained by the ion-slicing and wafer bonding technology. The quantum well active region grown on this Si-based InP film shows a superior photoemission efficiency, and it is found to be 65% as compared to its bulk counterpart.

INTRODUCTION

The increasing demands on a huge amount of data acquisition and processing have advanced the rapid development of next generation optoelectronic devices with fast response, large bandwidth, precision, and energy efficiency among others. It is well known that III-V compounds are direct band gap semiconductors, and they can act as active materials for light emission, which is impossible for traditional silicon material. Moreover, III-V semiconductors possess extremely high electron mobility and excellent nonlinear optical properties, i.e., the second and third optical susceptibility.[1] The heterogeneous integration of III-V compound semiconductors onto the conventional silicon substrate, forming a unique heterogeneous material platform, has emerged as one of the most promising materials for the advanced device applications in the field of integrated photonics and high speed electronics.[2,3] The continued pressure on the device performance motivates the development of a new technology of fabricating wafer-scale III-V compound semiconductors integrated onto silicon with high yield.

However, III-V compound semiconductors exhibit strong lattice and thermal mismatch with Si.[1,4] These incompatibilities strongly limit the quality of III-V compound semiconductor layers epitaxially grown on Si.[5,6] Alternatively, the combination of dissimilar semiconductor materials can be realized by using the ion-slicing technology that was developed by Bruel in 1995 and has been extensively applied to the mass production of silicon-on-insulator (SOI).[7] Additionally, the feasibility to fabricate compound semiconductors, e.g., SiC, InP, and GaAs, on Si has been demonstrated.[8–10] Generally, the defects introduced by ion (H, He) implantation will form the platelets filled with gas (H_2, He), which will grow and coalesce to form a micro-crack during annealing.[11] When the pressure inside of the micro-crack is strong enough to deform the surface, blisters will appear on the surface. With a stiffener intentionally bonded onto the wafer surface, the fracture of the whole layer will occur paralleled to the surface during annealing.[12] For the ion-slicing process, the direct wafer bonding is critical to achieve high-quality integrated wafers. Direct wafer bonding refers to the direct adhesion of two wafers with a sufficiently clean and preferably almost ideally mirror-polishing surface instead of using gluing layers. It is also a key technology in various processes, especially for microelectromechanical systems (MEMS) devices and hybrid integration in silicon photonics.[13–16]

The performance and reliability of devices based on the heterogeneously integrated materials strongly rely on the quality of the bonding interface. Therefore, it is necessary to obtain a perfect bonding interface without any defects after the post-bonding annealing. However, the bubble generation is a serious problem for direct wafer bonding.[17,18] In particular, the bubbles at the bonding interface occur frequently and become significantly serious as the wafer sizes increased. It has been classified that the main origins of the bubbles at the Si–Si bonding interface are the chemical reaction products and the decomposition of organic contamination on wafer surface.[17] The mechanism of Si-to-SiO_2 hydrophilic wafer bonding has been investigated in detail.[19–21] Conventionally, the bonding process takes place at room temperature, and the wafer surfaces are adhered together by 2-3 monolayers of water molecules and the polar OH groups, which terminate both the native and thermal SiO_2 by van der Waals type hydrogen bonds. During the post-annealing process, the OH molecules on the surfaces come sufficiently close to form covalent bonds between the wafer surfaces with water as the reaction product as follows:[20]

$$\mathrm{Si{-}OH + OH{-}Si \rightarrow Si{-}O{-}Si + H_2O}. \quad (1)$$

With enough water molecules at the bonding interface, reaction (1) is reversible when the annealing temperature is below 425 °C.[22] Therefore, the excess water molecules have to be removed in order to achieve strong siloxane bonds (Si–O–Si) across the bonding surface. Part of the water molecules diffuse along the bonding interface to outside, but it is a slow process. Part of the water molecules may also diffuse through the native or thermal oxide layer to react with bulk silicon to form silicon oxide and hydrogen as follows:[23]

$$\mathrm{Si + 2H_2O \rightarrow SiO_2 + 2H_2}. \quad (2)$$

The great amount of the gas from the bonding reaction, desorption of water molecules at the bonding interface and the decomposition of organic contamination on the wafer surface during annealing, causes a high internal pressure, subsequently resulting in the local de-bonding, i.e., the formation of interface bubbles.[24] The bonding reaction products are inevitable for hydrophilic wafer bonding and are impossible to be inhibited fundamentally. Fortunately, for Si–Si wafer bonding, the interfacial bubbles can be suppressed by high temperature (T > 800 °C) post-annealing since the native or thermal oxide becomes viscous.[24] However, the high temperature annealing (>800 °C) is not feasible for wafer bonding of most III-V compound semiconductors and Si, e.g., InP–Si wafer bonding, due to the large thermal expansion coefficient mismatch and potential thermal degradation or decomposition of compound semiconductors.[24,25] Furthermore, the little gas existing in the bonding interface of InP and Si or the oxide layer below the InP thin film could result in the bubbles due to the low stiffness of the InP thin film with a thickness of ~670 nm. Due to those complications, it is urgent to develop an efficient process to prevent the formation of bubbles at the bonding interface between III-V compound semiconductors and Si.

In this study, highly efficient lateral outgassing trenches (LOTs) were introduced to suppress the bubble formation at the InP–Si bonding interface. A proof-and-concept experiment has been conducted between the InP semiconductor and Si. The underlying mechanism of bubble formation at the bonding interface between the crystalline InP film and the Si substrate was analyzed. The relationship between bubble formation and the design of LOTs was described by a thermodynamic model. The efficiency of LOTs to inhibit bubbles only depends on the geometrical design instead of material properties. Hence, introducing LOTs is a promising solution to overcome the bubble problem in hydrophilic wafer bonding for heterogeneous materials. Thanks to LOTs, a high-quality bubble-free 2-in. Si–InP heterogeneous substrate was successfully fabricated, on which the grown quantum well (QW) demonstrated efficient photoluminescence (PL).

EXPERIMENTAL

In our studies, 2-in. epi-ready semi-insulating InP (100) wafers and 4-in. epi-ready Si (100) substrates covered with a 500 nm-thick thermal SiO_2 layer were used. For the investigation of the InP/SiO_2/Si bonding interface, the InP wafers were directly bonded with the Si substrates after N_2 plasma activation by using the EVG 301 wafer bonder. With N_2 plasma activation, the surface oxidation of InP wafers, which is inevitable with O_2-plasma activation, can be avoided.[26] Additionally, the bonding strength between InP and Si with N_2 plasma activation is higher than that with O_2-plasma activation in low plasma density.[27] The bonding interfaces were characterized by Scanning Acoustic Microscopy (SAM, PVA-Tepla SAM400) and x-ray photoelectron spectroscopy (XPS, Thermo Fisher 250 SI). For the fabrication of the Si–InP heterogeneous substrate, the InP wafers were co-implanted with He and H ions at room temperature using the Nissin EXCEED 2300RD ion implanter. In order to avoid the channeling effects, deliberate misalignment from the wafer normal of 7° was performed during the ion implantation processes. LOTs with different spacing (S) and dimensions (D) were fabricated on the SiO_2 layer on top of the Si substrates via the standard UV photolithography process. After that, 2-in. InP films were split and transferred onto the Si substrates with and without LOTs by the

ion-slicing technology, as reported previously.[28] The surface morphology of the InP film was characterized using an optical microscope (OM, Leica DM4000M). The LOT's structure was characterized by scanning electron microscopy (SEM, Zeiss Supra55). The qualities of the transferred InP films and bonding interfaces were examined by JEOL 2100F field-emission high resolution transmission electron microscopy (HRTEM) and selected area electron diffraction (SAED). The Raman spectra of the InP thin film on the trench region and non-trench region were excited by using a 514.5 nm laser using the Horiba Scientific LabRAM HR. The quantum wells (QWs) (200 nm $In_{0.52}Al_{0.48}As$/15 nm $In_{0.53}Ga_{0.47}As$/200 nm $In_{0.52}Al_{0.48}As$) were grown on both the Si–InP heterogeneous substrate and InP epi-ready substrate by molecular beam epitaxy (MBE) with Thermo VG Semicon V90. The photoluminescence (PL) spectroscopies of the QWs were characterized by using Thermo Scientific NICOLET iS50R FT-IR.

RESULTS AND DISCUSSION

The process flow for the heterogeneously prepared integrated InP film on the Si substrate using the ion-slicing technology is shown in Fig. 1(a). First of all, the 2-in. InP wafer was co-implanted with He and H ions at room temperature. After the surface activation with N_2 plasma, the implanted InP wafer and the Si (100) wafer were bonded at room temperature. After annealing at 150 °C for 1 h, the InP film is split from the InP wafer and transferred onto the Si substrate, and the InP/SiO_2/Si substrate was formed. In order to enhance the bonding strength between the InP film and the Si substrate, the obtained InP/SiO_2/Si substrate was further annealed at 300 °C for 30 min. During the annealing process, both the InP/Si bonding pair and the obtained InP/SiO_2/Si substrate were placed horizontally in the annealing furnace without applying any external pressure. Figure 1(b) shows a typical image of the Si–InP heterogeneous substrate, in which a 2-in. InP thin film with a thickness of around 500 nm has been successfully transferred onto a 4-in. Si substrate without introducing the LOT's structure. The surface of the transferred InP thin film was inspected, as shown in Fig. 1(c), and dense tiny bubbles appear on the surface of the InP thin film. As a reference, the epi-ready InP wafer was directly bonded with the Si substrate without LOTs after N_2 plasma treatment. The SAM analysis was performed to evaluate the bonding interface between InP and Si at room temperature or after annealing at 300 °C for 30 min, as shown in Figs. 1(d) and 1(e), respectively. It is clear that the dense tiny bubbles homogeneously distribute over the whole InP–Si bonding interface at room temperature. This suggests that the bubble formation is irrelevant to the ion implantation and thermal decomposition of organic contaminants at the bonding interface. After a low-temperature annealing at 300 °C for 30 min, it seems that the tiny bubbles disappear, while there is an irregular large bubble marked as A in Fig. 1(e). Moreover, a de-bonding area was observed in the peripheral region of the InP–Si bonding pair, as shown in Fig. 1(e). During the annealing process, the tiny bubbles grew up and merged together. The pressure inside the bubbles is defined as P_b, and the bonding strength is defined as P_s. If $P_b < P_s$, the bubble will be confined at the interface and continually grow up. If $P_b > P_s$, the de-bonding is triggered, which results in the large bubble and the de-bonding area.

In order to clarify the source of gas trapped in bubbles, XPS was employed to characterize the surface composition of the as-received InP wafer and the de-bonded InP wafer. The XPS profiles of the InP wafers are depicted in Fig. 2(a), and the binding energy was calibrated to the C 1 s photoemission peak of adventitious hydrocarbons at 285.0 eV. The corresponding deconvoluted spectra show

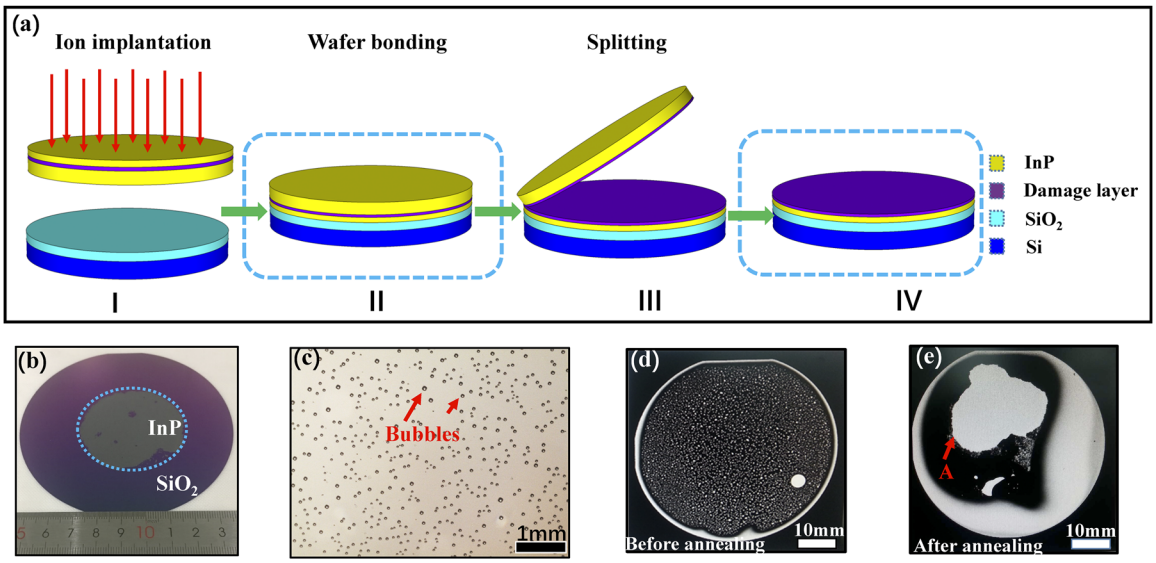

FIG. 1. (a) The process flow for the integration of the InP film on the Si substrate using ion-slicing technology. (b) The photo of a 2-in. InP film transferred onto a 4-in. Si substrate. (c) The OM image of the InP film surface. [(d) and (e)] SAM images of bonding quality at room temperature and after post-bonding annealing at 300 °C for 30 min, respectively.

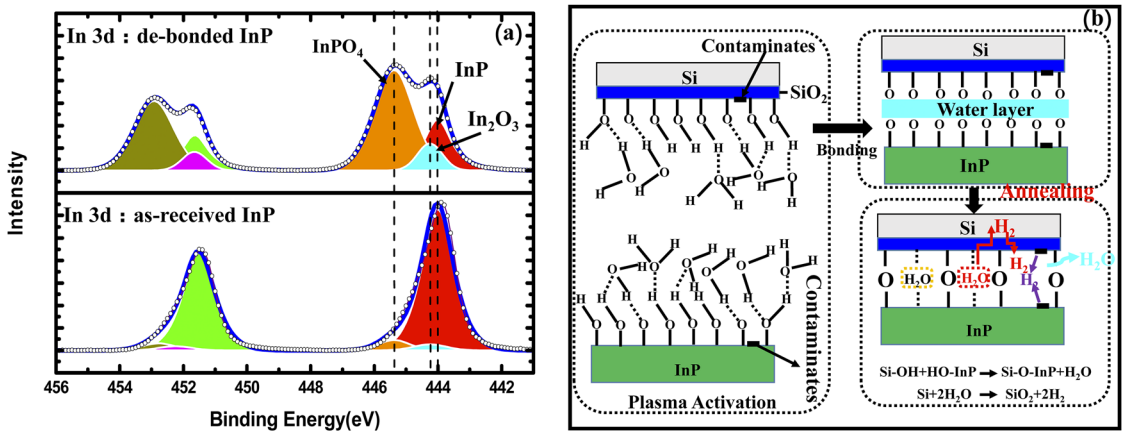

FIG. 2. (a) XPS spectrum of In 3d5/2 for the as-received and de-bonded InP wafer. (b) The schematic drawing of the mechanism of the InP-to-Si wafer bonding.

contributions from InP (at ~444 eV), In_2O_3 (at ~444.3 eV), and $InPO_4$ (at ~445.3 eV).[29–31] The InP component is dominant for the as-received InP wafer. However, the contents of $InPO_4$ and In_2O_3 drastically increase on the de-bonded InP wafer surface, which is accompanied by the reduction of the InP component. The growth of the oxide layer is coincident with the case of the Si/SiO_2 hydrophilic wafer bonding process.[32] It is well known that plasma surface activation results in broken dangling bonds of molecules on the surfaces of Si and SiO_2. The dangling bonds react instantaneously with water molecules, and silanol groups (Si–OH) are formed, which render the surface hydrophilic and are beneficial for the hydrophilic wafer bonding.[19] The similar process may also occur in InP–Si wafer bonding, as schematically shown in Fig. 2(b). After N_2 plasma activation treatment, the surfaces of InP and Si are very hydrophilic so that the water molecules are adsorbed on the surface easily. During the bonding process at room temperature, the Si and InP wafers are adhered together via the few monolayers of water molecules and the polar OH groups, which terminate thermal SiO_2 and InP by van der Waals type hydrogen bonds. After annealing at a high temperature, hydrogen bonds between InP–OH and Si–OH groups on bonded hydrophilic surfaces convert to InP–O–Si covalent bonds by the following reaction:

$$\text{Si–OH} + \text{OH–InP} \rightarrow \text{Si–O–InP} + H_2O. \quad (3)$$

Moreover, the water molecules may also diffuse through the thermal oxide and react with bulk silicon to form silicon oxide and hydrogen as reaction (2). Based on the InP-to-Si bonding mechanism, it is speculated that most of the gas trapped in the InP film bubbles comes from bonding reaction products, i.e., H_2, and desorption of water molecules at the bonding interface.

Due to the complicated causes of the gas trapped in bubbles at the interface, it is very hard to suppress the gas generation, in essence, during the hydrophilic wafer bonding process. Alternatively, the suitable "drainage" pipelines can be introduced to facilitate the generated gas diffusing out of the bonding interface. Hence, in order to verify the effect of the "drainage" pipelines, S = 500 μm and D = 2 μm LOTs were patterned to half area of the thermal SiO_2 layer on the Si substrate. The depth of the LOTs is about 250 nm, which is enough for gas diffusing outside. A 2-in. InP thin film was then transferred onto the patterned Si substrate by the ion-slicing technology, as schematically shown in Fig. 3(a). The InP thin film is divided into two parts by a red dashed line, i.e., trench and non-trench region, respectively. The LOTs are only located on the trench region. Figure 3(b) shows the picture of the fabricated InP thin film on the patterned Si substrate. It is clear that a lot of bubbles appear on the non-trench region, while sporadic bubbles exist on the trench region. The surface morphology of the InP thin film on the trench and the non-trench region was inspected by using an OM, as

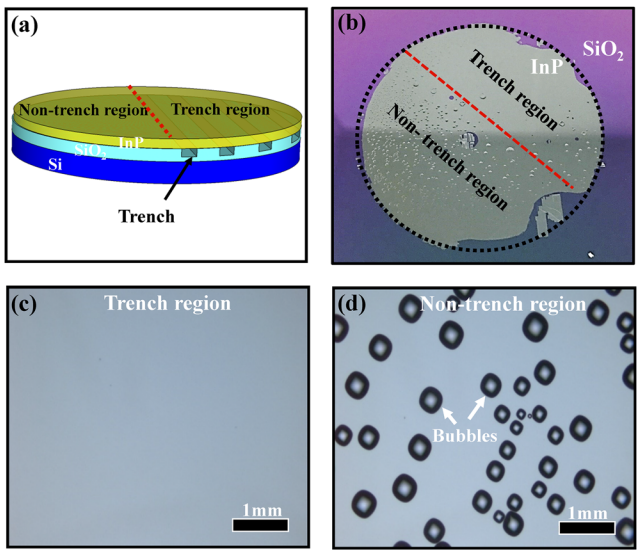

FIG. 3. (a) The schematic of the InP-on-patterned Si structure. (b) The photo of the 2-in. InP film transferred onto the Si substrate with a half-area patterned. The OM images of the surface morphology of the InP film (c) on the trench and (d) non-trench region, respectively.

shown in Figs. 3(c) and 3(d), respectively. Evident reduction in bubble density down to nearly zero is visible on the trench region, while a great number of uniformly distributed bubbles still exist on the non-trench region. Moreover, the bubble density on the non-trench region slightly decreases toward the trench region. Therefore, it is evident that the LOTs are highly effective to create the bubble-free Si–InP heterogeneous substrate by facilitating the gas to diffuse out of the bonding interface.

In order to study the outgassing efficiency of LOTs, the patterns with different S (S = 200 μm, 500 μm and 1 mm) and D (D = 2 μm and 8 μm) were designed on Si substrates. The InP thin films were transferred onto the patterned Si substrates by the ion-slicing technology. Figure 4 shows the process flow for the transferring process. The photos and OM images of InP thin films (highlighted with white dashed circles) transferred onto the patterned Si substrates are demonstrated in Fig. 5. Increasing the LOTs' spacing S from 200 μm to 500 μm, the surface of InP films is flat and smooth for both D = 2 μm and 8 μm, and bubble-free InP thin films were obtained. However, increasing the LOTs' spacing S up to 1 mm, a small number of bubbles appear and unevenly distribute on the surface of InP thin films with D = 2 μm and D = 8 μm. Increasing LOTs' spacing S, i.e., decreasing the trench density, greatly reduces the possibility for the gas of the bonding interface migrating to LOTs. In the case of S = 1 mm, the density and dimension of the bubbles are similar for D = 2 μm and 8 μm. It is indicated that the effect of LOTs' dimension D on the outgassing efficiency is much smaller than that of LOTs' spacing S. Therefore, LOTs' spacing S is the primary influence factor for outgassing. It is noted that the overall bonding yield is around 50%, as indicated in Fig. 5, caused by the unsatisfied surface cleanliness of Si substrates after the lithography process and InP substrates after the ion implantation process, which is limited by the cleaning process in our lab. It is believed that the overall bonding yield can be increased by improving the surface cleanliness of both Si and InP.

In order to clarify the relationship between bubbles and the design of LOTs, a thermodynamic model was proposed referring to the thermodynamic model for the interface bubbles in the bonded silicon wafers. Based on the thermodynamic model,[33] the Gibbs free energy ΔG can be expressed as

$$\Delta G = W(r) + \Gamma(r) + E_{elastic}(r, \Delta p), \tag{4}$$

where $W(r)$ is the external potential energy due to the volume increase of bubbles, namely,

$$W(r) = -\Delta p V_{bubble}, \tag{5}$$

where $\Delta p = p_i - p_{outside}$ (p_i is the pressure in the bubble and $p_{outside}$ is the outside pressure) and V_{bubble} is the volume of the bubble.

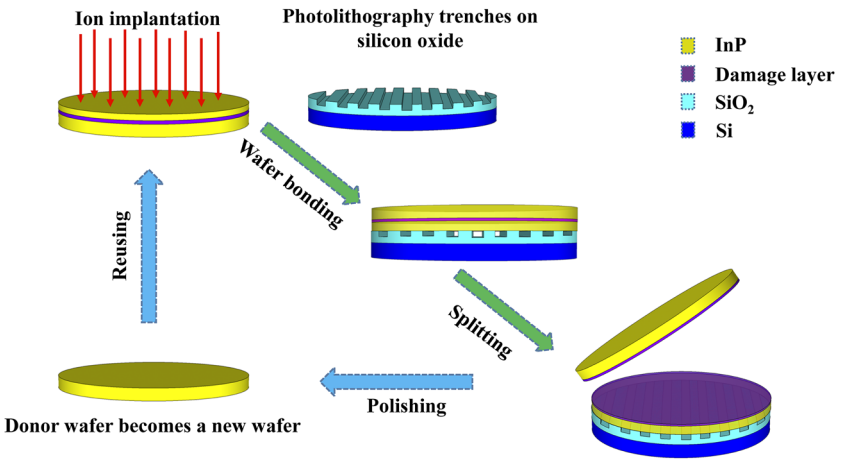

FIG. 4. The process flow for the transferring process of the InP film on a patterned Si substrate.

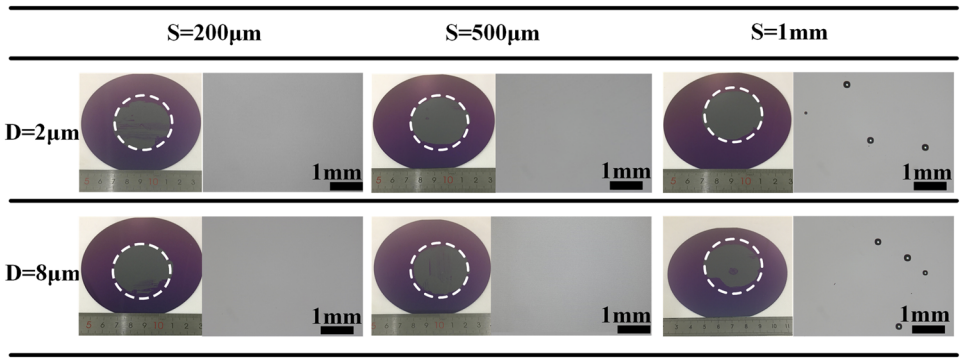

FIG. 5. The photos and OM images of the InP film transferred onto the patterned Si substrates with variable S (S = 200 μm, 500 μm and 1 mm) and D (D = 2 μm and 8 μm).

Assuming that the shape of the bubble is approximated by a cone with the height of h, as shown in Fig. 6(a), V_{bubble} can be derived as

$$V_{bubble} = \pi\alpha r^2 h, \tag{6}$$

where α is a geometrical factor of about 1/3-1/2 and r is the radius of the bubble. Γ(r) is the interface energy, namely,

$$\Gamma(r) = \pi\gamma r^2, \tag{7}$$

where γ is the interface energy per unit area.

The relation of the h, Δp, and r of the bubble is as follows:

$$h = \frac{\Delta p r^4}{64D}, \tag{8}$$

where D is the flexural rigidity of the InP film, namely,

$$D = \frac{Et^3}{12(1-v^2)}, \tag{9}$$

where E is the Young's modulus, which is 84 GPa for InP, t is the thickness of the InP thin film, which is 670 nm, and v is Poisson's ratio of InP, which is 0.36.

$E_{elastic}(r, \Delta p)$ is the elastic energy, namely,

$$E_{elastic}(r, \Delta p) = \frac{1}{2}\pi\alpha r^2 h \Delta p. \tag{10}$$

Thus, the Gibbs free energy becomes

$$\Delta G = -\frac{1}{2}\Delta p\pi\alpha r^2 h + \pi\gamma r^2 = -\frac{\Delta p\pi\alpha r^6}{128D} + \pi\gamma r^2. \tag{11}$$

In the case of InP/Si wafer bonding, the bonding energy normally exceeds the bulk fracture energy so that it is hard to obtain the interface energy. Therefore, γ is estimated to be the fracture energy of 0.75 J/m^2.[4] Due to the thin InP film, the difference in pressure between the inside and outside of the bubble is not very large. In experiments, the radii (r) of bubbles are in the range of 150 nm–600 nm and the heights (h) of bubbles are in the range of 50 nm–100 nm. According to Eqs. (8) and (9), Δp was estimated to be around about 1 atm. Therefore, p_i is 2 atm based on $\Delta p = p_i - p_{outside}$, where $p_{outside}$ is the atmospheric pressure (1 atm). With α = 1/3,[33] the Gibbs free energy is expressed as

$$\Delta G(erg) = -3.38 \times 10^4 r^6 + 23.56 r^2. \tag{12}$$

The red line in Fig. 6(c) shows the plot of the Gibbs free energy ΔG as a function of radius r of the bubble. With an increase in r, ΔG first increases and then decreases, reaching a maximum at the critical radius r_c. When $r < r_c$, since $\partial\Delta G/\partial r > 0$, the bubbles are not stable and will shrink away. However, once $r \geq r_c$, ΔG is decreasing with an increase in r, and bubbles can grow.

It is assumed that there is a certain area contributed to the generation and growth of one bubble. In order to cover all the surface area, the shape of the certain area is defined as a square, such as area A or B, surrounded by dashed line in Fig. 6(b). The gas molecules on the surface of area A diffuse and aggregate into one bubble, and the area B contributes to another bubble. An ideal gas law can be obtained as

$$p_i V_{bubble} = N_{bubble} KT, \tag{13}$$

where N_{bubble} is the number of molecules in one bubble, K is Boltzmann's constant (1.38×10^{-16} erg/K) and T is the absolute annealing temperature. In general, the size of the bubble is much smaller than the surrounding area. In the case of one period of LOTs, the dimension of the effective area contributed to the bubbles is smaller than LOTs' S, therefore, the area of A is defined as $A = S^2$. Based on the reaction (3), it is assumed that only the H_2O molecules of the bonding reaction products diffuse into the bubbles, and the molecules density per unit area is approximately equal to the atom density per unit area (C) on InP (100). Hence, the N_{bubble} is derived as

$$N_{bubble} = CS^2. \tag{14}$$

The ideal gas law can be expressed as follows:

$$p_i V_{bubble} = CS^2 KT. \tag{15}$$

Therefore, we can obtain the relation of LOTs' S as the radius r of the bubble,

$$S = \left(\frac{p_i \pi\alpha\Delta p}{64DCKT}\right)^{\frac{1}{2}} r^3. \tag{16}$$

When p_i = 2 atm, Δp = 1 atm, C = 5.8×10^{12}/mm^2, and T = 423.15 K,

$$S = 630.56 r^3. \tag{17}$$

The relation of LOTs' S and the radius r is plotted by the blue line in Fig. 6(c). When the $r = r_c$, LOTs' S corresponds to a critical value S_c = 1.2 mm. With the $S < S_c$, the number of gas molecules

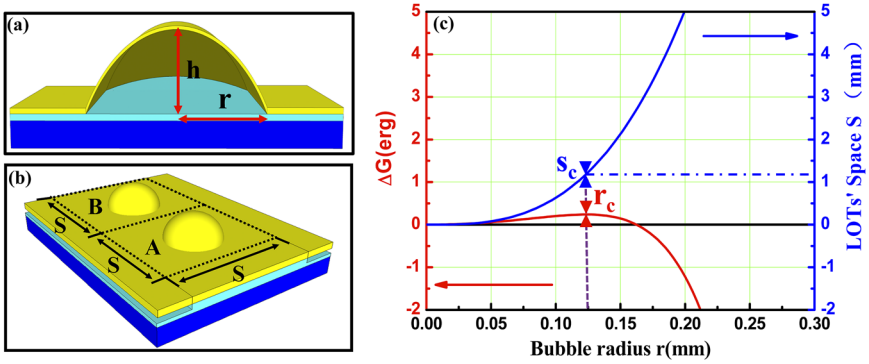

FIG. 6. (a) The sectional schematic drawing for the bubble. (b) The schematic drawing of certain square area A contributed to the generation and growth of one bubble and square area B contributed to another bubble. (c) The plot of Gibbs free energy ΔG and LOTs' space S as radius r of the bubble.

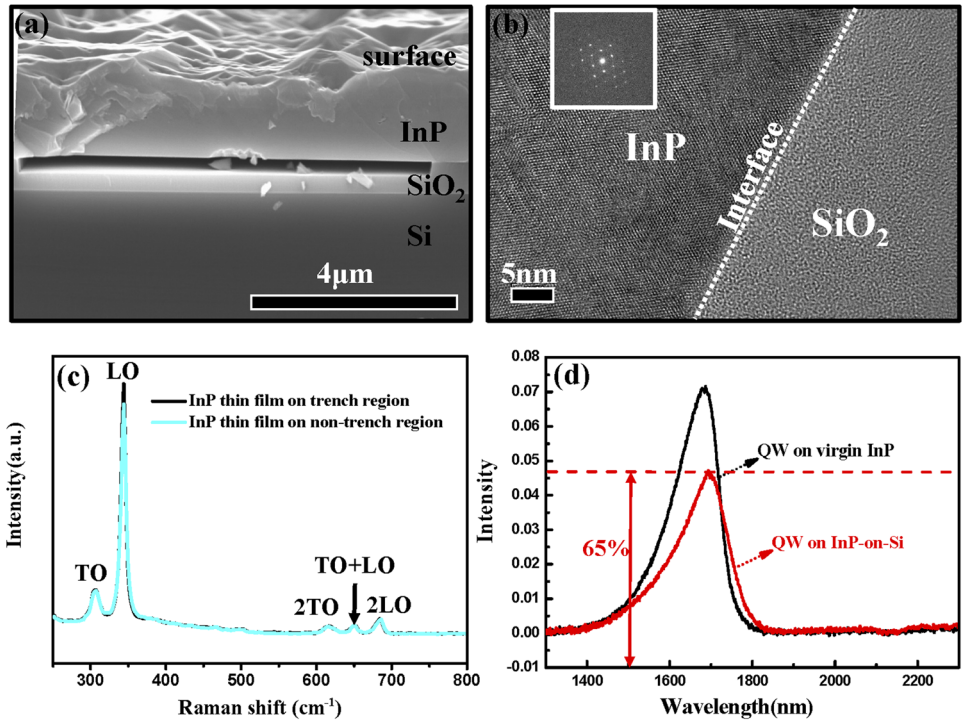

FIG. 7. (a) The sectional SEM image of the LOT's structure. (b) The sectional HTEM image of the Si–InP heterogeneous structure with the inset of SAED. (c) The Raman spectra of the InP thin film on the trench region and the non-trench region. (d) The PL spectra of the QW (200 nm $In_{0.52}Al_{0.48}As$/15 nm $In_{0.53}Ga_{0.47}As$/200 nm $In_{0.52}Al_{0.48}As$) grown on the Si–InP heterogeneous substrate with LOTs and the virgin InP substrate, respectively.

produced in the effective area is not enough for the generation and growth of one stable bubble. It is almost coincident with the results of our experiments in Fig. 5(b). However, some bubbles appear on the surface when S = 1 mm in our experiments, which might be due to the fact that the gas molecules in the bubbles not only come from the bonding reaction products but also due to the desorption of water molecules at the bonding interface.

According to the design of LOTs, the 2-in. bubble-free InP thin film has been transferred onto a patterned Si substrate (D = 8 μm and S = 500 μm). Figure 7(a) shows a cross-sectional SEM image of the InP thin film on the LOT. The InP thin film is completely suspended over the LOT without any cracks. The quality of the InP film and the bonding interface was evaluated by HRTEM and SAED. The HRTEM image in Fig. 7(b) shows that the InP thin film is a high-quality single crystal film, corresponding to regular diffraction spots in the SAED pattern in the inset. There is a distinct and perfect bonding interface between the InP thin film and the thermal SiO_2 layer. The LOTs do not affect the qualities of the InP thin film and bonding interface, as indicated by the similar Raman spectra of the InP thin film on the trench region and non-trench region shown in Fig. 7(c). The typical first-order TO and LO modes were found to be 306.9 cm^{-1} and 344.6 cm^{-1}, respectively, for the InP thin film on both trench and non-trench regions.[34] The TO mode is very weak in comparison with the LO mode since it is forbidden in the backscattering configuration on a (100) face. The second-order 2TO, TO + LO, and 2LO modes measured at 617 cm^{-1}, 650 cm^{-1}, and 682 cm^{-1}, respectively, are in good agreement with the expected 2TO (Γ), TO (Γ) + LO (Γ), and 2LO (Γ) phonons.[34] Anyhow, there is no significant difference in the Raman spectra of the InP thin film on the trench and non-trench regions, which suggests the uniform quality of the InP thin film with LOTs. In order to evaluate the photoluminescence properties of the Si–InP heterogeneous substrate with the LOT's structure, the same QW (200 nm $In_{0.52}Al_{0.48}As$/15 nm $In_{0.53}Ga_{0.47}As$/200 nm $In_{0.52}Al_{0.48}As$) was grown on both the Si–InP heterogeneous substrate and the InP substrate by MBE. The PL spectra of the QW in Fig. 7(d) show that the PL intensity of the QW grown on the Si–InP heterogeneous substrate reaches about 65% of that grown on the InP substrate. It indicates that it is promising to achieve photonic devices on the Si–InP heterogeneous substrate with LOTs.

CONCLUSIONS

In conclusion, the highly effective LOTs have been introduced to obtain a bubble-free wafer-scale Si–InP heterogeneous substrate. Based on the analysis of chemical compositions at the bonding interface, it is found that the same chemical reactions in the InP–Si bonding process occur as the reactions in Si–Si bonding. The nucleation and aggregation of products of gas molecules at the bonding interface cause the InP film to deform to form the bubbles. The gas molecules can be effectively limited by the design of LOTs. LOTs' spacing S plays a dominant role in the outgassing efficiency. Based on the experimental and thermodynamic analysis, it is suggested that the outgassing efficiency of LOTs will not be enough to remove the bubbles when the LOTs' spacing S exceeds the critical value S_c. The 2-in. wafer-scale bubble-free Si–InP heterogeneous substrate was successfully achieved by the introduction of LOTs. The LOT's structure does not have an adverse effect on the qualities of the InP film and the bonding interface. Furthermore, the quality of the InP

thin film on the whole wafer is consistent, whether on the trench region and non-trench region. Therefore, the whole area of the Si–InP heterogeneous substrate can be used to fabricate the devices. The photoluminescence of the InGaAs/InAlAs QW grown on the Si–InP heterogeneous substrate reaches 65% of its counterpart on InP substrates. The mechanism of the LOTs to facilitate gas diffusion out of the bonding interface is a physical effect, only depending on the design of the LOTs. Hence, it is promising to inhibit the formation of bubbles at the bonding interface for all III-V compound semiconductors integrating with the Si substrate by wafer bonding.

AUTHOR'S CONTRIBUTIONS

J. L. and T. Y. contributed equally to this work.

ACKNOWLEDGMENTS

This work was supported by the National Key RD Program of China (Grant No. 2017YFE0131300), the National Natural Science Foundation of China (Grant Nos. U1732268, 61874128, 11622545, 61851406, and 11705262), the Frontier Science Key Program of CAS (Grant No. QYZDY-SSW-JSC032), the Chinese–Austrian Cooperative R&D Project (Grant No. GJHZ201950), the Shanghai Science and Technology Innovation Action Plan Program (Grant No. 17511106202), the Program of Shanghai Academic Research Leader (Grant No. 19XD1404600), the Shanghai Sailing Program (Grant Nos. 19YF1456200 and 19YF1456400), and the K. C. Wong Education Foundation (Grant No. GJTD-2019-11).

DATA AVAILABILITY

The data that support the findings of this study are available from the corresponding author upon reasonable request.

REFERENCES

[1] O. Moutanabbir and U. Gösele, Annu. Rev. Mater. Res. **40**, 469 (2010).
[2] K. K. Samanta and D. Kissinger, IEEE Microwave Mag. **18**, 14 (2017).
[3] M. Madsen, K. Takei, R. Kapadia, H. Fang, H. Ko, T. Takahashi, A. C. Ford, M. H. Lee, and A. Javey, Adv. Mater. **23**, 3115 (2011).
[4] D. Pasquariello, M. Camacho, K. Hjort, L. Dózsa, and B. Szentpáli, Mater. Sci. Eng.: B **80**, 134 (2001).
[5] D. S. Wuu, R. H. Horng, and M. K. Lee, J. Appl. Phys. **68**, 3338 (1990).
[6] H. Itakura, T. Suzuki, Z. K. Jiang, T. Soga, T. Jimbo, and M. Umeno, J. Cryst. Growth **115**, 154 (1991).
[7] M. Bruel, Electron. Lett. **31**, 1201 (1995).
[8] J. Grisolia, F. Cristiano, B. De Mauduit, G. B. Assayag, F. Letertre, B. Aspar, L. Di Cioccio, and A. Claverie, J. Appl. Phys. **87**, 8415 (2000).
[9] R. Singh, I. Radu, R. Scholz, C. Himcinschi, U. Gösele, and S. H. Christiansen, Semicond. Sci. Technol. **21**, 1311 (2006).
[10] I. Radu, I. Szafraniak, R. Scholz, M. Alexe, and U. Gösele, Appl. Phys. Lett. **82**, 2413 (2003).
[11] J. Grisolia, G. Ben Assayag, A. Claverie, B. Aspar, C. Lagahe, and L. Laanab, Appl. Phys. Lett. **76**, 852 (2000).
[12] N. Daghbouj, N. Cherkashin, F.-X. Darras, V. Paillard, M. Fnaiech, and A. Claverie J. Appl. Phys. **119**, 135308 (2016).
[13] V. Dragoi, E. Pabo, J. Burggraf, and G. Mittendorfer, Microsyst. Technol. **18**, 1065 (2012).
[14] B. Szelag, K. Hassan, L. Adelmini, E. Ghegin, P. Rodriguez, F. Nemouchi, P. Brianceau, A. Schembri, D. Carrara, P. Cavalié, F. Franchin, M. C. Roure, L. Sanchez, C. Jany, and S. Olivier, IEEE J. Sel. Top. Quantum Electron. **25**, 1 (2019).
[15] T. Dinh, H. P. Phan, N. Kashaninejad, T. K. Nguyen, D. V. Dao, and N. T. Nguyen, Adv. Mater. Interfaces **5**, 1800764 (2018).
[16] T. Yamashita, S. Hirata, R. Inoue, K. Kishibe, and K. Tanabe, Adv. Mater. Interfaces **6**, 1900921 (2019).
[17] X. X. Zhang and J. P. Raskin, J. Microelectromech. Syst. **14**, 368 (2005).
[18] M. M. R. Howlader, F. Zhang, and M. G. Kibria, J. Micromech. Microeng. **20**, 065012 (2010).
[19] S. H. Christiansen, R. Singh, and U. Gosele, Proc. IEEE **94**, 2060 (2006).
[20] T. Plach, K. Hingerl, S. Tollabimazraehno, G. Hesser, V. Dragoi, and M. Wimplinger, J. Appl. Phys. **113**, 094905 (2013).
[21] Q.-Y. Tong and U. M. Gösele, Adv. Mater. **11**, 1409 (1999).
[22] C. Wang, Y. Liu, and T. Suga, ECS J. Solid State Sci. Technol. **6**, P7 (2017).
[23] U. Gösele, Q.-Y. Tong, A. Schumacher, G. Kräuter, M. Reiche, A. Plößl, P. Kopperschmidt, T.-H. Lee, and W.-J. Kim, Sens. Actuators, A **74**, 161 (1999).
[24] D. Liang and J. E. Bowers, J. Vac. Sci. Technol., B **26**, 1560 (2008).
[25] S. N. G. Chu, C. M. Jodlauk, and W. D. Johnston, Electrochem. Soc. **130**, 2398 (1983).
[26] D. Pasquariello and K. Hjort, IEEE J. Sel. Top. Quantum Electron. **8**, 118 (2002).
[27] S. Kondo, T. Okumura, R. Osabe, N. Nishiyama, and S. Arai, in *22nd International Conference on Indium Phosphide Related Mater* (IEEE, 2010).
[28] J. Lin, T. You, M. Wang, K. Huang, S. Zhang, Q. Jia, M. Zhou, W. Yu, S. Zhou, X. Wang, and X. Ou, Nanotechnology **29**, 504002 (2018).
[29] L. L. Kazmerski, P. J. Ireland, P. Sheldon, T. L. Chu, S. S. Chu, and C. L. Lin, J. Vac. Sci. Technol. **17**, 1061 (1980).
[30] J. C. C. Fan and J. B. Goodenough, J. Appl. Phys. **48**, 3524 (1977).
[31] M. Faur, M. Faur, D. T. Jayne, M. Goradia, and C. Goradia, Surf. Interface Anal. **15**, 641 (1990).
[32] P. Amirfeiz, S. Bengtsson, M. Bergh, E. Zanghellini, and L. Börjesson, J. Electrochem. Soc. **147**, 2693 (2000).
[33] K. Mitani and U. M. Giisele, Appl. Phys. A: Solids Surf. **54**, 543 (1992).
[34] L. Artús, R. Cuscó, J. M. Martín, and G. González-Díaz, Phys. Rev. B **50**, 11552 (1994).